

LA-UR -80-3012

UNIVERSITY OF CALIFORNIA

**MASTER**

**TITLE:** Seismograms of Explosions at Regional Distances in the Western U. S.: Observations and Reflectivity Method Modeling

**AUTHOR(S):** Kenneth H. Olsen, G-7  
Lawrence W. Braile, Purdue Univ. & G-Div. Consultant

**SUBMITTED TO:** Proceedings Volume of the NATO Advanced Study Institute: "Identification of Seismic Sources - Earthquake or Underground Explosion." (Held 8 - 18 September 1980, Oslo Norway)

DISCLAIMER  
The U.S. Government is authorized to reproduce and distribute reprints for Government purposes not withstanding any copyright notation that may appear hereon.

University of California

By acceptance of this article, the publisher recognizes that the U.S. Government retains a nonexclusive, royalty free license to publish or reproduce the published form of this contribution, or to allow others to do so, for U.S. Government purposes.

The Los Alamos Scientific Laboratory requests that the publisher identify this article as work performed under the auspices of the U.S. Department of Energy.



**LOS ALAMOS SCIENTIFIC LABORATORY**

Post Office Box 1663 Los Alamos, New Mexico 87545

An Affirmative Action/Equal Opportunity Employer

DISTRIBUTION OF THIS DOCUMENT IS UNLIMITED

**SEISMOGRAMS OF EXPLOSIONS AT REGIONAL DISTANCES IN THE WESTERN  
UNITED STATES: OBSERVATIONS AND REFLECTIVITY METHOD MODELING**

**K. H. Olsen<sup>1</sup> and L. W. Braile<sup>2</sup>**

**1 Geosciences Division, Los Alamos Scientific  
Laboratory, Los Alamos, New Mexico 87545, U.S.A.**

**2 Geoscience Department, Purdue University,  
West Lafayette, Indiana 47907, U.S.A.**

**ABSTRACT.** Seismic energy propagating through vertically and laterally varying structures of the earth's crust and lower lithosphere-uppermost mantle is responsible for the numerous and complex seismic phases observed on short-period seismograms at regional distance ranges (100 to 2000 km). Recent advances in techniques for computing synthetic seismograms make it practical to calculate complete seismograms that realistically model many features of regional phases. A modified reflectivity method program is used to interpret some details of record sections of Nevada Test Site (NTS) underground explosions that were observed 700 to 800 km from the sources.

**I. INTRODUCTION**

Regional seismic phases recorded by high-gain, short-period or broadband instruments are likely to play an increasingly important role in seismic source location and identification as acceptable magnitude thresholds are pushed to lower levels. From the standpoint of complexity of seismograms, the epicentral distance range between ~200 km and the transition to simpler teleseismic waveforms around 2000 km presents many challenges to the seismic analyst. In this range, propagation paths can traverse the crust, the lower lithosphere, and the uppermost mantle where both vertical and lateral heterogeneities strongly influence waveform characteristics. Good observational data are rare for testing analysis techniques developed for regional problems. In contrast to the numerous detailed crustal refraction/reflection profiles that have been obtained from many parts of the world out to distances ~200 km, relatively few

long-range profiles exist where station spacing is sufficiently tight to facilitate a clear interpretation of the onset, development, and amplitude vs. distance behavior of the many observable phases. Thus, although signals from sources of interest may be easily observable at regional distances, derivation of source parameters from observations at sparsely located observatories or arrays will require careful analysis and modeling of the intricacies of wave propagation at these scales.

Phases of interest in regional identification studies fall into two main categories: large amplitude, long duration, but somewhat indistinct wave groups such as Lg and  $\bar{P}$ ; and body waves (mainly compressional) that appear either as first arrivals or closely following as possible wide angle reflections/near-critical refractions from interfaces and/or steep velocity gradients in the deep crust, lower lithosphere, and uppermost mantle. The Lg and  $\bar{P}$  phases are often the largest amplitude features on regional seismograms, but a clear explanation of how Lg and  $\bar{P}$  propagate is still lacking [1]; this lack perhaps is reflected in the fact that the  $\bar{P}$  phase is sometimes inappropriately called Pg in the literature. The group velocities (~3.5 km/s for Lg, ~6.0 km/s for  $\bar{P}$ ) imply that Lg ( $\bar{P}$ ) propagates as shear (compressional) waves multiply reflected within the crust--which may thus act as a waveguide. Some authors [2] prefer to treat Lg as a superposition of higher mode Love and Rayleigh waves propagating in a nearly laterally homogeneous, vertically layered crust. In any case, the propagation physics is complicated and will require quite sophisticated synthetic seismogram codes to properly model and interpret observed waveforms.

Record sections of long-range seismic refraction profiles often show one or more nearly parallel travel time (T) vs. distance ( $\Delta$ ) branches following within several seconds of first arrivals [3, 4, 5]. Each secondary branch may be traceable only over a distance interval of 50 to 200 km before being replaced with another branch or set of arrivals [5, 6]. These are usually interpreted as parts of cusp phases arising from critical refractions and/or wide-angle reflections from first order discontinuities or steep velocity gradients in the upper mantle. Archambeau et al. [7] and Burdick and Helmberger [8], for example, have derived velocity vs. depth models for the major features of the upper mantle beneath the U.S. by a joint analysis of travel times, amplitude vs. distance variations, and waveform fitting of the first few compressional arrivals observed at widely separated seismograph stations throughout the U.S. These and similar models by others are most valid for depths greater than about 250 km. Although these analyses suggest that the main features of mantle structure at depths below about 300 km

(corresponding to compressional first arrivals at epicentral ranges beyond 1500 km) may be more uniform over a global scale [8], it is known that significant lateral variations in lower lithosphere and uppermost mantle properties occur beneath the continents on regional and perhaps even finer scales [8, 9, 10, 11]. In the depth range between the Moho and 300 km, several types of structural variations have been suggested in the literature that would give rise to wide angle reflections, converted phases, and similar closely spaced arrivals on seismograms at regional ranges. These include the presence or absence of the S-wave and/or the P-wave low velocity zone (LVZ) in the athenosphere, high velocity mantle lids [12, 13], alternating lamellae of positive and negative velocity gradients [6], etc. These early arriving phases often have better defined onsets than the P and Lg phases and, since they are observed at distances beyond that where a true head wave Pn arrival can be expected, they may be useful in regional source location and identification. In order to make use of the information contained in these arrivals (especially the amplitude vs. distance behavior for particular paths of interest), it will be necessary to use modern sophisticated synthetic seismogram techniques to derive localized fine scale details from generalized crust-mantle models.

The purpose of this paper is to explore a few of the problems in modeling regional short-period seismograms by means of a modified reflectivity method [14] computer program developed by R. Kind [15]. This numerical program accounts for the effects of a buried source and is thus capable of computing 'complete' seismograms--including surface reflected body waves and surface waves. The effects of anelastic attenuation (Q) for each layer are included as an integral part of the method [15]. The most severe limitation of the technique for studies of regional seismograms is the assumption of lateral homogeneity (this is also a limitation for normal modes summation techniques). An item of interest will be the extent synthetics can be made to match observed waveforms under this restriction.

Two problems are considered. The first, labeled the B-3 model for brevity, employs a simple model consisting of three layers in the crust without velocity gradients and an almost uniform velocity mantle. A large range of apparent surface phase velocities is used in order to display S phases and surface waves. The second calculation, the A-10 model, treats the mantle structure in detail, but confines attention to compressional phases near their start of the seismogram. The more important conclusions of the A-10 model are summarized here--a fuller discussion of this calculation and the implications for uppermost mantle structure beneath the western U.S. can be found in a previous publication [16].

A comparison of the synthetic seismogram calculations has been made with a 100-km-long record section of short-period vertical component seismograms obtained in eastern Idaho during the 1978 Yellowstone-Eastern Snake River Plains (Y-ESRP) seismic profiling experiment. For these observations, the sources were underground nuclear explosions at the Nevada Test Site (NTS) at distances between 720 and 820 km from the nearly radially oriented linear station array (Fig 1). Only the records from the largest NTS explosion, the  $m_b = 5.7$  RUMMY event at 1720:00.076 GMT, 27 September 1978, are reproduced here since they have the best signal-to-noise ratio of the three NTS explosions observed during the experiment. Additional details of the Y-ESRP instrumentation, experiment, and data can be found elsewhere [16].

## 2. COMPUTATIONAL TECHNIQUE

As discussed by Kind [15] and by Fuchs and Müller [14], the reflection coefficient and time shift calculations are carried out in the frequency domain and then Fourier transformed to plot seismograms. We included Müller's [17] earth flattening approximation in both of our problems to account for earth curvature effects. Both P and S velocities are independently specified in all calculations, since the reflection coefficients are functions of both P and S velocity contrasts at non-normal incidence angles and are required even when only computing P phases over a narrow time window. In the A-10 calculation, for example, the departure of the P/S velocity ratio in a layer from that given by Poisson's ratio = 1/4 is an important factor in our interpretation [16]. Densities are given by a Birch's Law relation (density =  $0.252 + 0.3788 * P$  velocity). The attenuation factor  $Q_\alpha$  for P waves was chosen as 25 in the source layers, 200 in the upper crust, and 1000 in the lower crust and the uppermost mantle layers; for the LVZ modeling of the A-10 model,  $Q_\alpha$  in the athenospheric layers was adjusted as part of the fitting procedure (see Fig. 5). The attenuation factor for S waves was always assumed to be  $4Q_\alpha/9$ . The explosive source algorithm [16] was used with the source buried at a depth of 0.640 km in a layer of P velocity = 3.55 km/s. These were close to actual field values for the NTS RUMMY explosion. Time intervals, number of samples, and computed lengths of seismograms were chosen so that the dominant frequency of the source spectrum was 1.6 Hz for the A-10 calculation--again close to the observed value. In order to save computer time for the extended duration B-3 seismogram sections, the parameters were chosen so that the dominant frequency of the source was shifted to 0.25 Hz; although this was low, we felt it was adequate for the purposes of this initial study. To avoid long computer runs, the wave field was only computed within a limited phase velocity window:

1 km/s to 20 km/s for B-3, and 6.5 km/s to 1000 km/s for A-10. These integration limits sometimes introduced spurious single cycle "phases" at these apparent velocities in the computed record sections. The limit velocities were chosen so as to not overlap or interfere with arrivals of interest in the observations. In the record section plots, the amplitudes of each trace have been multiplied by station distance to maintain a convenient scaling of the spreading phases.

### 3. DISCUSSION

#### 3.1 The Extended Time Seismograms: B-3 Model

Figure 2 is a true relative amplitude vertical component record section of the RUMMY explosion recorded on ten matched short-period (1 Hz natural frequency) instruments deployed in the eastern Snake River Plains (Fig. 1). Although the time scale is too compressed to reveal many details of the waveforms, several important overall features can be noted. The broad (~40-second-long) envelope of the  $\bar{P}$  phase appears at reduced times between approximately 30 to 60+ seconds, and is the largest amplitude feature on the record. In contrast, the Lg phase expected at reduced times of ~130+ seconds (an average velocity of about 3.5 km/s) is poorly developed on these unfiltered records; it is only obvious at the 770-km station. A few impulsive arrivals can be seen (such as the first arrivals at reduced time ~10 seconds, which will be discussed in Sec. 3.2, and perhaps an Sn [ ] phase at  $t_{red} \sim 80$  seconds and  $\Delta > 780$  km), but the impression one gets by viewing this observed section is that the correlations seem to be better described as broad energy correlations rather than phase correlations. A similar conclusion is suggested by seismograms from central Asia shown in the paper of Ruzaikin et al. [1]. A coherent structure in the  $\bar{P}$  and Lg phases is difficult to trace from station to station even though the stations are only separated by 8 km on the average.

The results of an attempt to model late time arrivals over a regional distance range is shown in Fig. 3. A rudimentary, almost trivial, crust/mantle velocity structure was assumed that consisted of three constant velocity layers in the crust overlaying a nearly constant velocity halfspace. (A slight negative gradient in P velocity was introduced just below the Moho in order to suppress the Pn amplitudes as required by the observations; see Sec. 3.2.) We note several points.

(a) The seismogram section from 100 to 900 km and the enlarged individual record for 800 km shows a surprising amount of complexity at times beyond the first arrivals even though an extremely simple earth model and source function is used. Groups corresponding to the  $\bar{P}$  and Lg phases can be identified.

- (b) There appears to be a considerable amount of S-wave energy although none is present in the explosion source algorithm. This is probably due to P-to-J and S-to-P, etc., conversions at interfaces and to multiples the program adequately includes.
- (c) The calculated dispersed fundamental mode Rayleigh wave is very large. There are at least two reasons this Rayleigh wave is not representative of the observations. First, no corrections for the short-period bandpass response of the seismometers were included in the synthetics. Second, because of limitations on computer time and storage, the assumed source spectrum has too much energy at the longer periods, over enhancing the Rayleigh waves. Long-period Rayleigh waves from actual underground explosions are probably generated or enhanced by mechanisms such as spall closure and/or tectonic strain release; these mechanisms are not treated by the explosion algorithm used for the present calculation.
- (d) Because the calculated seismograms are quite complicated even for this simple earth model, they give the impression of "energy correlation" rather than phase correlation for at least the  $\bar{P}$  and Lg phases as was the case with the observations in Fig. 2. In order to better understand the gross behavior of these phases with distance and to identify the origin of obscure features, it will be necessary to include calculations of the horizontal (radial) component.

These results suggest that the modified reflectivity method, even with the restrictive assumption of lateral homogeneity, can be a useful technique in understanding the intricacies of Lg and P phases and the types of earth structures that most affect them. Parameter studies would help identify those aspects where refinements due to lateral heterogeneity and/or scattering need to be considered in order to better match observations.

### 3.2 Early Time Arrivals: A-10 Model

Figures 4a and 4b are enlarged portions of the first seconds of the digitized RUMMY vertical component seismograms (see also Fig. 2) that show details of the earliest arrivals. We have interpreted [16] this record section in terms of three different compressional phases, all having apparent velocities close to 8 km/s: (a) an extremely weak leading arrival labeled  $P_n$ , which was lost in the background noise for the two other, lower yield, NTS shots that were also recorded during the Y-ESRP experiments; (b) a stronger phase labeled  $P_{1id}$  follows  $P_n$  by about two or three seconds for epicentral distances between 700 and 780 km; (c) beyond 780 km, the  $P_{1id}$  phase appears to be overtaken and overwhelmed by a low-frequency phase,  $P_1$ , whose amplitude increases rapidly with distance out to at least the farthest

station of the linear array. The detailed reasons for these labels and identifications are discussed in [16]; they can be summarized as follows.

The phase labeled  $P_n$  could be a wide angle reflection from a weak P-velocity contrast in the lower lithosphere below the Moho rather than a true headwave (in the strict sense of the mathematical definition) that travels along the M-discontinuity interface over the entire 800-km path. However, since the sub-Moho P velocity (7.7 to 7.9 km/s) in this region of the Great Basin is known to be close to both the average and the apparent velocity observed in Figs. 2 and 4, plus the fact that other travel time arguments [16] suggest there is no evidence for mantle lids or other thin but fairly high gradient zones down to a depth of about 100 km, argues that the most straightforward explanation for this arrival is that it is a  $P_n$ -type phase. The energy at 800 km is greatly reduced because the wave travels in a region beneath the Moho that has a slight but negative gradient.

The sudden onset at about 780 km and subsequent rapid amplitude growth of the  $P_1$  phase indicates it is the cusp of the critically refracted P-waves from the steep velocity gradient at the base of the athenospheric low velocity zone. The observed dominant low frequency content is then easily explained by the attenuation of the high frequency components as the energy travels first downward and then back up through the very low-Q region of the LVZ. The notation of  $P_1$  for this phase follows the convention established by Archambeau et al. [7].

The travel times, moderate amplitudes, and relatively high frequency content imply the phase identified as  $P_{lid}$  is a wide angle reflection from a discontinuity near the base of the mantle lid (= top of LVZ) in this area.

The conclusions concerning these three early arriving compressional phases summarized above were confirmed by using the modified reflectivity program to quantitatively model the arrival times, amplitudes, and waveforms in the first 15 seconds of the record sections. The procedure was to begin with a generic P-velocity vs depth model for the western U.S. (the T-7 model) derived from a wider data set by Burdick and Helmberger [8] and then to perturb the model to achieve a better fit [16]. Because of the influence of S-velocity contrasts on the P-wave reflectivity calculations, an S-velocity vs. depth model derived by Priestly and Brune [18] from an analysis of Rayleigh and Love wave dispersion on paths crossing the area of interest in the Great Basin of Eastern Nevada was incorporated into the synthetic modeling. The starting T-7 and Priestly-Brune velocity models



are shown by dotted lines in Fig. 5. The generic T-7 P-wave model has a pronounced mantle lid with a strong positive P-velocity gradient beneath the Moho for depths from 33 to 65 km. Calculation of synthetics for this lid structure gave very large amplitudes for the "P<sub>n</sub>" arrival, which was superimposed on a strong reflection from the base of the lid at 65 km [16]. Thus, the T-7/Priestly-Brune starting model gave results very different from observations. To bring the calculated synthetic seismograms into agreement with observations, the gradient at the base of the LVZ had to be raised to shallower depths and the positive gradient lid replaced with a smooth but gradual negative gradient starting at the M-discontinuity. The final model, A-10, that matches observations is shown by the solid lines in Fig. 5. Figure 6 is the comparison between the observed and synthetic record sections. Interestingly, no discontinuity in P-velocity is necessary to explain the P<sub>lid</sub> reflections; the reflections can be adequately modeled by a small negative step in S velocities at a depth of about 100 km. The synthetics, however, do not seem to adequately model the long oscillatory trains following the P<sub>1</sub> phase onset. This is probably due to interference effects caused by fine structure in the lower LVZ velocity gradient that we have not yet modeled by thin enough layers in the calculation [16].

These calculations illustrate that synthetic modeling techniques can be helpful in phase identification and in quantitative calculations of amplitude vs. distance behavior and waveform characteristics. With a sophisticated reflectivity method calculation we were able to model several important features of regional short-period seismograms. The technique appears promising in advancing knowledge of wave propagation and source identification at regional distance ranges.

#### ACKNOWLEDGMENTS

We especially thank Rainer Kind for making available to us the modified reflectivity method computer program that we have adapted for our analyses. Paul A. Johnson was responsible for the computer runs. The calculational and data reduction efforts for this research were supported by the U.S. Department of Energy and partially by ONR Earth Physics Program grant N00014-75-C-0972 to L.W.B. The Snake River Plains data were collected during research partially funded by the U.S. National Science Foundation (grant EAR-77-23707 to the University of Utah and EAR-77-23357 to Purdue University) and by the U.S.G.S. Geothermal Exploration Program grant 14-08-0001-G-532 to Purdue.

#### FIGURE CAPTIONS

Fig. 1. (a) Location map of the western United States with relative positions of the Nevada Test Site and the Y-ESRP recording line. (b) Enlargement showing positions of stations that recorded the 27 September 1978 RUMMY explosion. Asterisk denotes approximate area for mantle ray turning points from NTS explosions.

Fig. 2. Low time resolution seismic record section of the RUMMY explosion as recorded at Snake River Plains stations. Upward ground motion to the left.

Fig. 3. (a) Synthetic seismogram vertical component record section calculated from the P and S velocity vs depth structure (Model B-3) shown in (b). (c) Expanded plot of the synthetic seismogram at the 800-km distance. Approximate arrival time and average velocity windows for different phases or groups are indicated.

Fig. 4. (a) True relative amplitude record section of early compressional arrivals from the RUMMY explosion. (b) Same as (a) with increased amplitudes to show weak  $P_n$  phase. Upward motion to the left. All traces bandpass filtered between 0 and 3 Hz.

Fig. 5. P-velocity ( $\alpha$ ) and S-velocity ( $\beta$ ) vs depth plots for the T-7/Priestly-Brune and A-10 models. Assumed Q structure at left;  $\sigma$  is Poisson's ratio.

Fig. 6. Comparison of the observed (a) record section with the synthetic section calculated from the A-10 model (b).

## REFERENCES

1. A. I. Ruzaikin, I. L. Nersesov, V. I. Khalturin, and P. Molnar, *J. Geophys. Res.* 82, pp. 307-316, 1977.
2. L. Knopoff, F. Schwab, K. Nakanishi, and F. Chang, *Geophys. J. R. astr. Soc.* 39, pp. 41-70, 1974.
3. V. Z. Ryaboi, *Izv. (Bull.) Acad. Sci. USSR, Geophys. Ser., AGU Trans.* 3, pp. 177-184, 1966.
4. R. P. Masse, *Bull. Seism. Soc. Am.* 63, pp. 911-935, 1973.
5. A. Hirn, L. Steinmetz, R. Kind, and K. Fuchs, *Z. Geophys.* 39, pp. 363-384, 1973.
6. R. Kind, *J. Geophys.* 40, pp. 189-202, 1974.
7. C. B. Archambeau, E. A. Flinn, and D. G. Lambert, *J. Geophys. Res.* 74, pp. 5825-5865, 1969.
8. L. J. Burdick and D. V. HelMBERGER, *J. Geophys. Res.* 83, pp. 1699-1712, 1978.
9. J. E. York and D. V. HelMBERGER, *J. Geophys. Res.* 78, pp. 1883-1886, 1973.
10. M. Cara, *Geophys. J. R. astr. Soc.* 57, pp. 649-670, 1979.
11. B. A. Romanowicz and M. Cara, *Geophys. Res. Lett.* 7, pp. 417-420, 1980.
12. A. L. Hales, *Earth and Planet. Sci. Lett.* 7, pp. 44-46, 1969.
13. D. P. Hill, *Geol. Soc. Am. Bull.* 83, pp. 1639-1648, 1972.
14. K. Fuchs and G. Müller, *Geophys. J. R. astr. Soc.* 23, pp. 417-433, 1971.
15. R. Kind, *J. Geophys.* 44, pp. 603-612, 1978.
16. K. H. Olsen, L. W. Brails, and P. A. Johnson, *J. Geophys. Res.*, submitted for publication 1980.
17. G. Müller, *J. Geophys.* 42, pp. 429-436, 1977.
18. K. Priestly and J. Brune, *J. Geophys. Res.* 83, pp. 2265-2272.

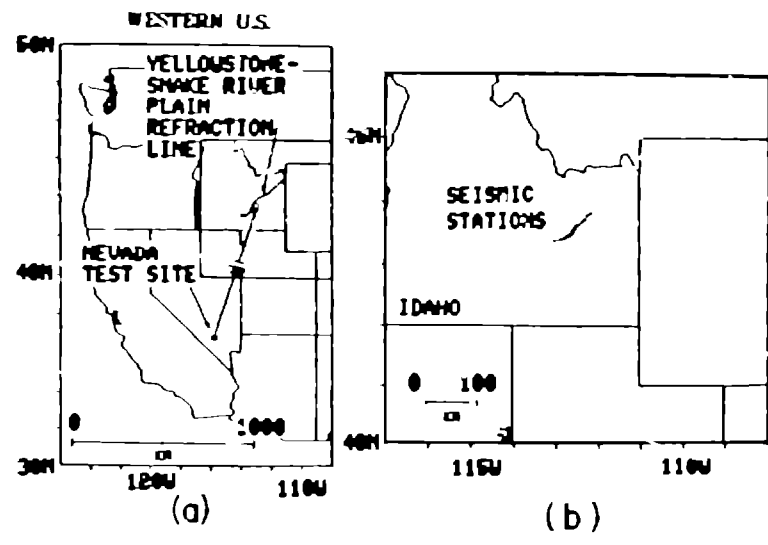


Figure 1

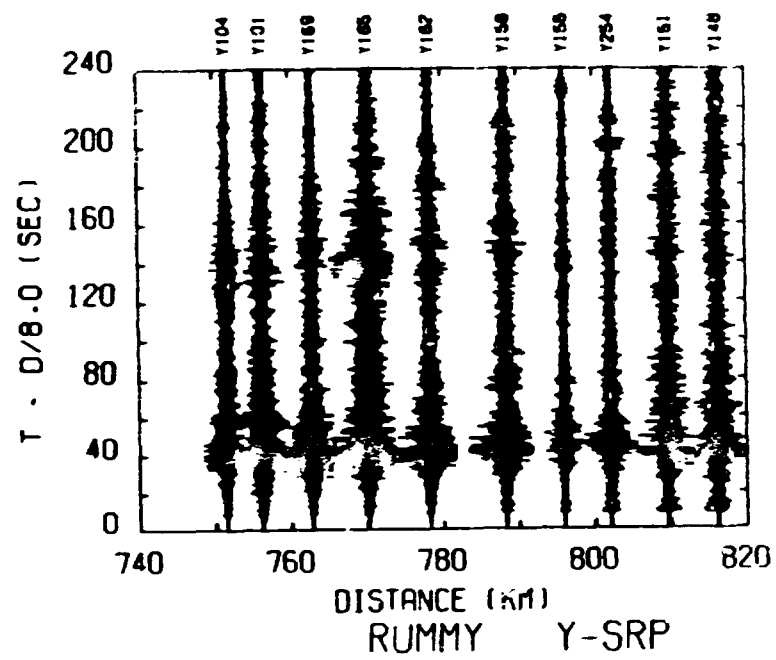


Figure 2

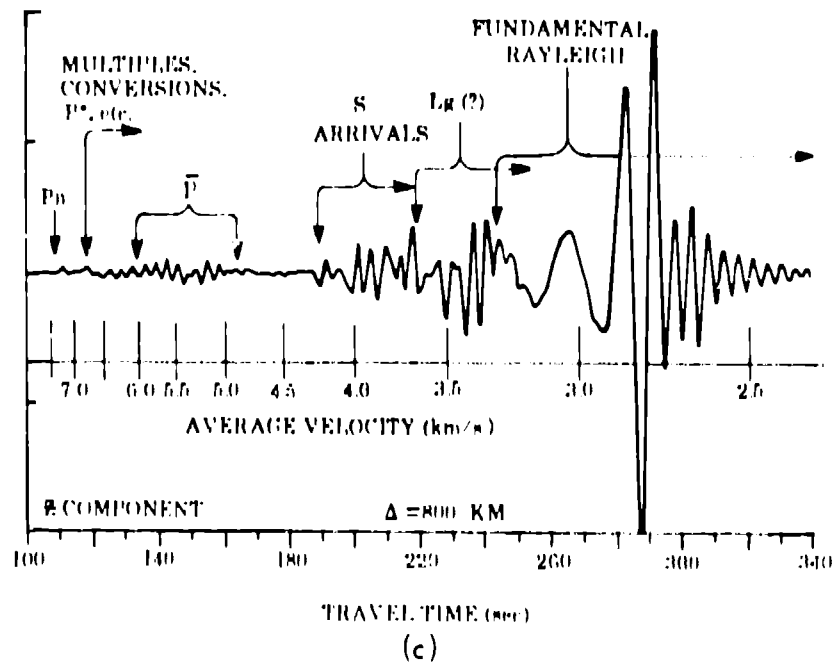
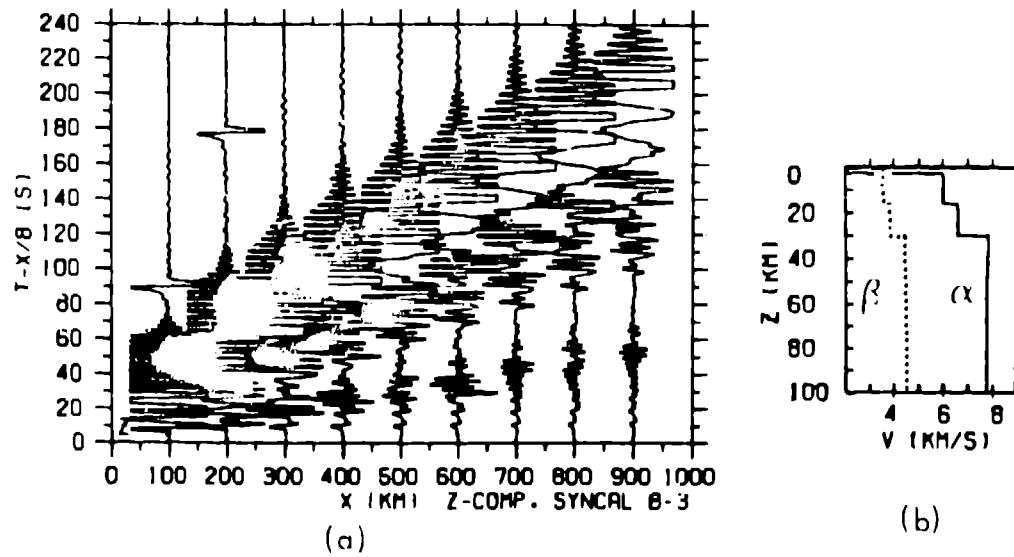


Figure 3

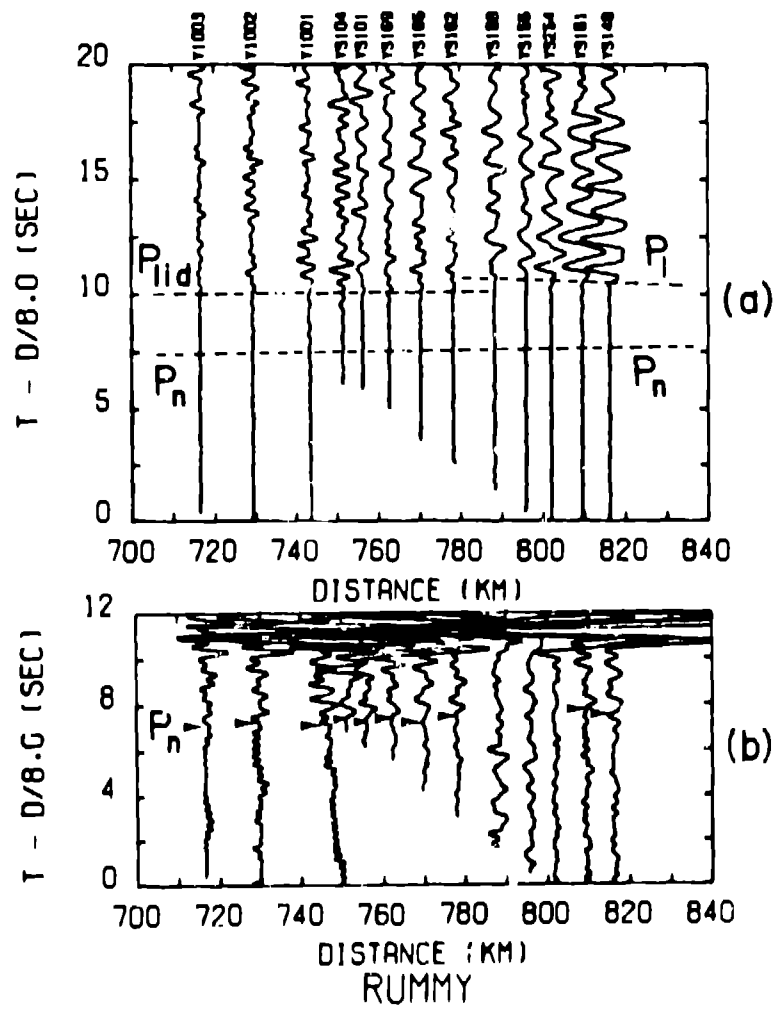


Figure 4

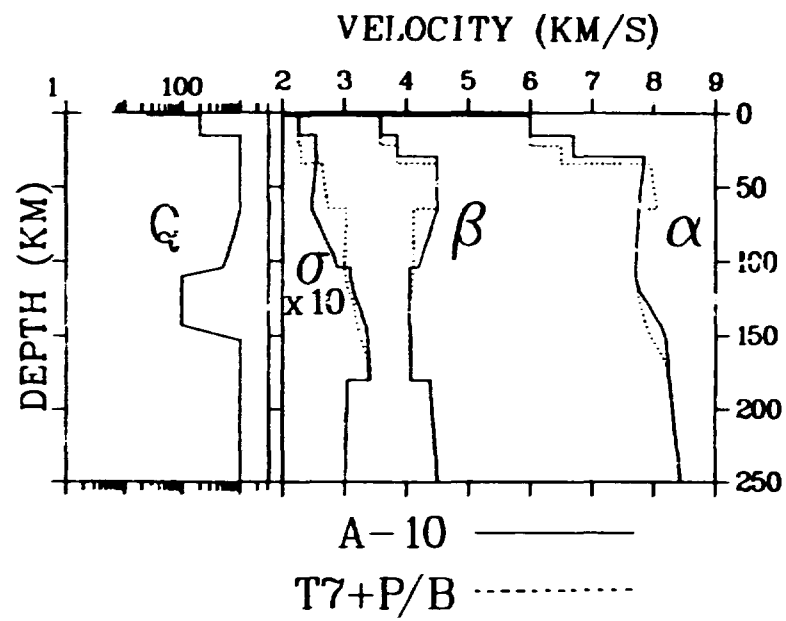
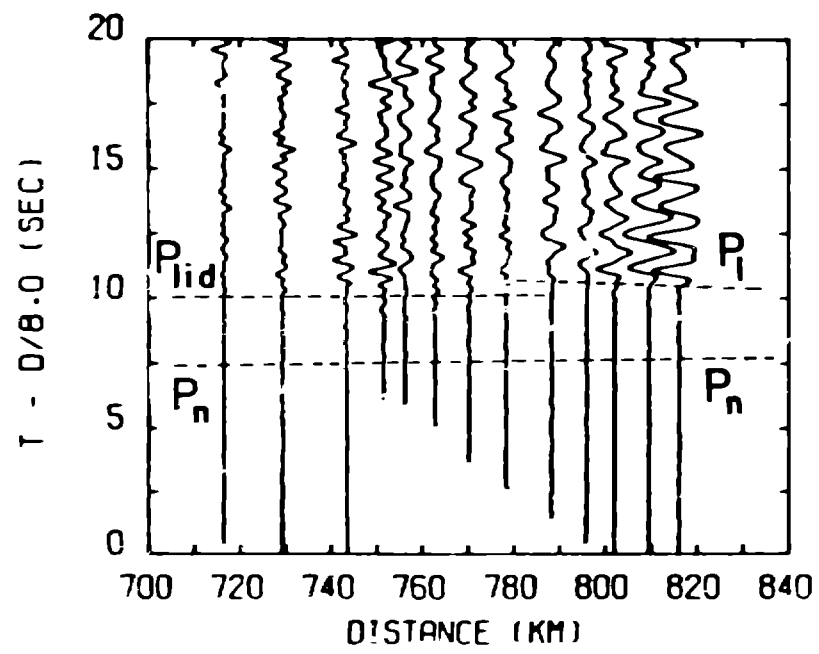
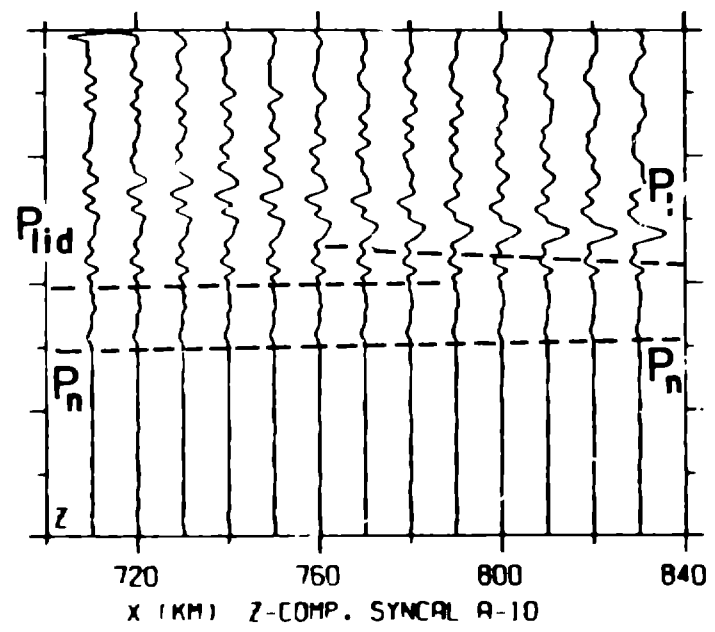


Figure 5





(a)



(b)

Figure 6